BIOPHYSICS

Difference in hydration structures between F-actin and myosin subfragment-1 detected by small-angle X-ray and neutron scattering

Tatsuhito Matsuo[1], Toshiaki Arata[2], Toshiro Oda[3] and Satoru Fujiwara[1]

[1]Quantum Beam Science Directorate, Japan Atomic Energy Agency, Tokai-mura, Naka-gun, Ibaraki 319-1195, Japan
[2]Department of Biological Sciences, Graduate School of Science, Osaka University, Toyonaka, Osaka 560-0043, Japan
[3]RIKEN SPring-8 Center, RIKEN Harima Institute, Sayo-gun, Hyogo 679-5148, Japan

Hydration structures around F-actin and myosin subfragment-1 (S1), which play central roles as counterparts in muscle contraction, were investigated by small-angle X-ray scattering (SAXS) and small-angle neutron scattering (SANS). The radius of gyration of chymotryptic S1 was evaluated to be 41.3±1.1 Å for SAXS, 40.1±3.0 Å for SANS in H_2O, and 37.8±0.8 Å for SANS in D_2O, respectively. The values of the cross-sectional radius of gyration of F-actin were 25.4±0.03 Å for SAXS, 23.4±2.4 Å for SANS in H_2O, and 22.6±0.6 Å for SANS in D_2O, respectively. These differences arise from different contributions of the hydration shell to the scattering curves. Analysis by model calculations showed that the hydration shell of S1 has the average density 10–15% higher than bulk water, being the typical hydration shell. On the other hand, the hydration shell of F-actin has the average density more than 19% higher than bulk water, indicating that F-actin has a denser, unusual hydration structure. The results indicate a difference in the hydration structures around F-actin and S1. The unusual hydration structure around F-actin may have the structural property of so-called "hyper-mobile water" around F-actin.

Key words: hydration shell, SAXS, SANS

Proteins in physiological conditions fluctuate constantly under the influence of thermal fluctuations of surrounding solvent molecules, the most abundant of which is water molecules. Proteins achieve their functions by changing their conformations utilizing this thermal energy of the solvent. Elucidation of interactions between proteins and water is thus indispensable for the ultimate understanding of protein functions. A first step toward this goal is to characterize the structural and dynamic properties of hydration water around proteins as well as proteins themselves. In this context, we have investigated the dynamic properties of the protein actin[1–3].

Actin forms a helical polymer (F-actin), and plays crucial roles in a variety of functions related to cell motility[4]. This multi-function of F-actin arises from flexibility of F-actin that enables it to interact with various actin-binding proteins. For understanding the origin of this flexibility and thereby the mechanism of the multi-functions, characterization of the structural and dynamic properties of F-actin including hydration water is required. In particular, investigation of hydration water around F-actin is important because it has been suggested that water plays an important role in chemomechanical energy transduction during muscle contraction[5,6]. Furthermore, the water molecules around F-actin has been suggested to have unusual properties (higher rotational mobility than bulk water), compared to usual hydration water that have lower rotational mobility than bulk water[6].

We employed small-angle X-ray and neutron scattering techniques to investigate the structural properties of hydration water around F-actin and myosin subfragment-1 (S1),

Corresponding author: Satoru Fujiwara, Quantum Beam Science Directorate, Japan Atomic Energy Agency, 2-4 Shirakata-Shirane, Tokai-mura, Naka-gun, Ibaraki 319-1195, Japan.
e-mail: fujiwara.satoru@jaea.go.jp

which is a proteolytic fragment of the myosin molecule containing a motor domain that interacts with actin in muscle contraction. Small-angle scattering arises from the difference in scattering density (the contrast) between the particles of interest and solvent. Signs and amplitudes of the contrasts of proteins and hydration water are different between small-angle X-ray scattering (SAXS), small-angle neutron scattering (SANS) in H_2O, and SANS in D_2O: in SAXS, the contrast of proteins in solution is positive and that of hydration water, assuming higher density than bulk water, is also positive; in SANS in H_2O, the contrast of proteins is positive, but that of hydration water is negative with small amplitudes; and in SANS in D_2O, the contrast of proteins is negative while that of hydration water is positive[7]. Utilizing these differences, combined analysis of the measurements by SAXS, SANS in H_2O, and SANS in D_2O provides information on the hydration structure of proteins[7].

The SAXS and SANS measurements were performed on F-actin in H_2O and D_2O to investigate the hydration structure. Similar measurements were also done on S1. Comparison of the results of F-actin and S1 indicates the denser hydration shell around F-actin than that around S1.

1. Materials and methods

1.1. Sample preparation

Actin was extracted from chicken breast muscle (pectoralis) and purified as described[8]. Further purification was done by gel filtration using a column (HiLoad 26/600 Superdex 200 pg; GE healthcare) in solution containing 5 mM Tris-HCl (pH 8.0), 0.2 mM ATP, 0.1 mM $CaCl_2$, 1 mM NaN_3, and 0.5 mM dithiothreitol (G-buffer), in which the actin molecules are monomeric (G-actin). To prepare the samples in D_2O, additional dialysis against the G-buffer in D_2O was performed. The F-actin samples were prepared by polymerization of G-actin by adding $MgCl_2$ to 1 mM[9] just before the scattering measurements. The protein concentration was determined spectrophotometrically by using the extinction coefficients, $E_{290}^{1\%}$ of 6.3 for G-actin and $E_{280}^{1\%}$ of 11.1 for F-actin.

S1 was prepared by chymotryptic digestion of myosin from rabbit skeletal muscle as described.[10] Purification of S1 obtained was done by gel filtration using a column (HiLoad 26/600 Superdex 200 pg; GE healthcare) in solution containing 20 mM Tris-HCl (pH 8.0), 150 mM KCl, 1 mM NaN_3, and 0.5 mM dithiothreitol. This chymotrypsin-treated S1, the molecular weight of which is 110 kDa, consists of the heavy chain (lacking the regulatory light chain-binding portion) and the essential light chain. The samples in D_2O were prepared by additional dialysis against the D_2O solution containing the same salt compositions as above. The concentration of S1 was determined spectrophotometrically by using $E_{280}^{1\%}$ of 7.5.

1.2. Small-angle scattering experiments

The SAXS measurements were carried out at the beamline BL45XU-SAXS at SPring-8, Hyogo, Japan, using incident X-rays with the wavelength (λ) of 1.0 Å. The measurements on a concentration series of the samples (F-actin in H_2O, F-actin in D_2O, S1 in H_2O and S1 in D_2O) between 1 mg/ml and 5 mg/ml were performed at the sample-to-detector distance of 2.5 m at 293 K. Two-dimensional SAXS patterns were measured with a PILATUS 300K-W detector (DECTRIS), then circularly averaged to obtain one-dimensional scattering curves using the program FIT2D[11]. Background subtraction was done using the program Primus[12] to obtain net scattering curves. Each scattering curve was obtained by accumulating three sets of scattering data from 500-ms exposure, during which no radiation-damage effects were observed.

The SANS measurements were carried out on the small-angle diffractometer D22 at the Institut Laue-Langevin, Grenoble, France, using neutrons with $\lambda = 6$ Å ($\Delta\lambda/\lambda = 10\%$). The measurements were done at the sample-to-detector distance of 5.6 m at 293 K. Exposure time was 10–20 min for each sample. Data reduction to obtain one-dimensional net scattering curves was carried out using the program GRASP[13].

1.3. Guinier analysis of the scattering curves

Guinier analysis[14] of the scattering curves was done to evaluate the radius of gyration (R_g) for S1 or the cross-sectional radius of gyration (R_c) for F-actin. The scattering curve, $I(Q)$, where Q (= $4\pi\sin\theta/\lambda$, where 2θ is the scattering angle) denotes the momentum transfer, can be approximated at the Guinier region ($QR_g < 1.3$[14]) of the scattering curves as,

$$I(Q) = I(0)\exp(-R_g^2 Q^2/3), \tag{1}$$

where $I(0)$ denotes the intensity at $Q = 0$. A linear fit to the Guinier plot (the plot of $\ln[I(Q)]$ versus Q^2) provides the values of R_g from the slope and $I(0)$ from the intercept at $Q = 0$.

For rod-like particles such as F-actin, the scattering curves have an approximate form,

$$I(Q) = I_c(Q)/Q, \tag{2}$$

where $I_c(Q)$ denotes the scattering curve of the cross-section of the particle. Since the Guinier region of $I_c(Q)$ can be approximated as,

$$I_c(Q) = I_c(0)\exp(-R_c^2 Q^2/2), \tag{3}$$

the R_c and $I_c(0)$ values can be evaluated from a linear fit to the cross-sectional Guinier plot (the plot of $\ln[QI(Q)]$ versus Q^2).

1.4. Model calculations

Further analysis was done by model calculations based on atomic models obtained by X-ray crystallography, X-ray

fiber diffraction (XFD), or three-dimensional reconstruction of electron microscopy (EM) images. For S1, the crystal structure of S1 prepared by papain digestion of myosin (PDB ID: 2MYS[15]) was used. The papain-treated S1 consists of the heavy chain, the essential light chain, and the regulatory light chain. The heavy chain forms the catalytic domain and the lever arm, which is a long stretch of α-helix of the heavy chain extending from the catalytic domain. The essential light chain and the regulatory light chain are wrapped around this α-helix of the heavy chain. The chymotrypsin-treated S1 used here, on the other hand, does not contain the regulatory light chain and its corresponding region in the heavy chain. The atomic model of papain-treated S1 was thus modified so that the C-terminal residues from Cys^{815} of the heavy chain and the regulatory light chain were removed. In addition, the missing side chains in the essential light chain in the crystal structure were added to the C^{α} coordinates manually. The extra methyl groups were also removed from the methylated lysine residues in the crystal structure. The missing residues in the crystal structure were complemented using a template-based loop structure prediction server ArchPRED[16].

The scattering curve calculated from the crystal structure of S1 was found not to fit well to the experimental curve regardless of the hydration shell (data not shown). A SAXS study on the myosin-family proteins, myosin V and VI, indeed showed that the structures of S1 in solution is different from those in crystals[17]. Global search of the structure of S1 thus needed to be performed. Since major structural changes have been shown to occur in the orientation of the lever arm relative to the catalytic domain[17,18], the global search of the lever arm orientation was performed. Each of three Euler angles describing the orientation of the lever arm (the residues 707–814 in the heavy chain and the essential light chain) around the residue Cys^{707} [19] was changed with a step of 30°, and for each orientation, the scattering curves were calculated using the programs CRYSOL and CRYSON[20]. CRYSOL and CRYSON include the contribution of the first hydration shell with a thickness of 3 Å in the calculation of scattering curves, taking the relative contrast to bulk water as a parameter. The global search was thus performed at various relative contrasts of the hydration shell. At each of the contrasts between 0% and 40% with a step of 1%, the global search of the orientation of the lever arm was performed to determine the model which fits simultaneously to the SAXS data, the SANS data in H_2O, and the SANS data in D_2O by minimizing the score function, P,

$$P = \chi^2_{SAXS} + \chi^2_{SANSH} + \chi^2_{SANSD},$$

$$\chi^2 = (1/(N-1)) \sum_{i=1}^{N} \{(I_{exp}(Q_i) - cI_{calc}(Q_i))/\sigma_{exp}(Q_i)\}^2, \quad (4)$$

where the subscripts SANSH and SANSD denote the SANS data in H_2O and the SANS data in D_2O, respectively, N is the number of the data points, $I_{exp}(Q_i)$ and $I_{calc}(Q_i)$ are the experimental and calculated scattering intensity at Q_i, respectively, c is the scale factor for the calculated curves, defined as $I_{exp}(0)/I_{calc}(0)$, and $\sigma_{exp}(Q_i)$ is the experimental error at Q_i. The fits were performed to the extrapolated scattering curves to zero protein concentration, obtained from a concentration series of the experimental scattering curves. In this manner, both the relative contrast of the hydration shell and the model of S1 can be determined.

For F-actin, three atomic models of the actin molecule obtained from XFD studies (PDB ID: 2ZWH[21]) and EM studies of F-actin (PDB ID: 3MFP[22] and 3G37[23]) were used. The F-actin models were constructed as 13-mers (for 2ZWH and 3MFP), or 12-mers (for 3G37) of the actin molecules from these models, assuming the left-handed 13/6 helical symmetry as was done previously[24]. Since these structures were based on the models obtained from the XFD or EM measurements of the "solution" samples, the structures should be free from the distorting molecular forces such as crystal-packing force. Thus, the structural search of the actin molecule in F-actin was not performed. At each of the relative contrasts of the hydration shell between 0% and 50% with a step of 1%, the scattering curves of the models for SAXS, SANS in H_2O, and SANS in D_2O were calculated using CRYSOL and CRYSON. The R_c values of the models were then obtained from the cross-sectional Guinier plots of these curves. The relative contrast of the hydration shell was determined so that the discrepancy between the experimental and calculated R_c values was minimized using the score function, S, defined as,

$$S = \xi_{SAXS} + \xi_{SANSH} + \xi_{SANSD},$$

$$\xi = \sqrt{\{(R_c^{exp} - R_c^{calc}(h))/\sigma_{exp}\}^2}, \quad (5)$$

where R_c^{exp}, σ_{exp}, and $R_c^{calc}(h)$ denote the experimental R_c, the standard deviation of R_c^{exp}, and the calculated R_c at the contrast of the hydration shell, h, respectively.

2. Results and discussion

2.1. Small-angle scattering experiments

Figure 1A and B shows examples of the Guinier plots of S1, and the cross-sectional Guinier plots of F-actin, respectively. Figure 1C and D shows the concentration dependences of the R_g values of S1 and the R_c values of F-actin, respectively. Linear extrapolation of these values to zero protein concentration provides the values at infinite dilution, which are devoid of distorting effects of the inter-particle interference. Although the isotopic effects of D_2O should not be observed in SAXS, the SAXS data of the samples in D_2O as well as in H_2O were measured because the inter-particle interference could be different between the particles in H_2O and those in D_2O. The obtained R_g and R_c values were, however, similar in H_2O and D_2O as shown in Figure 1C and D. Thus it was concluded that the differences between the SAXS data in H_2O and in D_2O are negligible
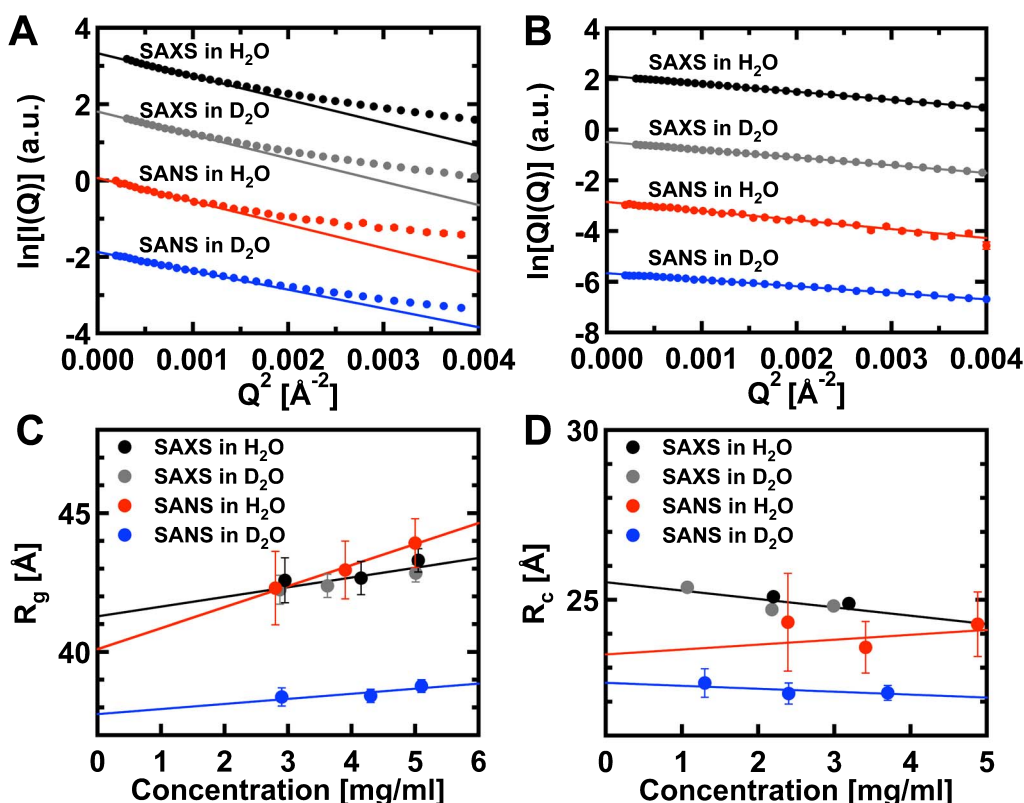
Figure 1   Examples of (A) the Guinier plots of chymotriptic S1, and (B) the cross-sectional Guinier plots of F-actin. In (A), the curves of SAXS in H_2O at 4.2 mg/ml (black), SAXS in D_2O at 5.0 mg/ml (gray), SANS in H_2O at 3.9 mg/ml (red), and SANS in D_2O at 4.3 mg/ml (blue) are shown. In (B), the curves of SAXS in H_2O at 2.2 mg/ml, SAXS in D_2O at 2.2 mg/ml, SANS in H_2O at 2.4 mg/ml, and SANS in D_2O at 2.4 mg/ml are shown. The color assignment is the same as in (A). Error bars are within symbols. The corresponding linear fits are also shown. The ranges for the linear fits were selected so that QR_g (or QR_c) < 1.3.[14] In (C) and (D) are shown concentration dependences of the R_g values of S1, and the R_c values of F-actin, obtained from the plots in (A) and (B), respectively, along with the linear fits to the data points.

both for S1 and F-actin, and the fits were done on the combined data.

The extrapolated R_g values of S1 and R_c values of F-actin are summarized in Table 1. The values obtained from SANS in D_2O were smaller than those from SANS in H_2O, which were then smaller than those from SAXS. This relationship is consistent with that which is expected if the hydration shell has higher density than bulk water[7]. The R_g values of S1 obtained here are consistent with the earlier SAXS studies[25,26] though the R_g value from SANS in D_2O is slightly smaller than the reported value of 40.0 ± 1.5 Å in the earlier SANS study[27]. The R_c values of F-actin are also consistent with the earlier SANS study[28] and SAXS studies[29,30].

Table 1   Summary of the values of R_g of S1 and R_c of F-actin.

	R_g of S1 (Å)	R_c of F-actin (Å)
SAXS	41.3 (1.1)	25.4 (0.03)
SANS in H_2O	40.1 (3.0)	23.4 (2.4)
SANS in D_2O	37.8 (0.8)	22.6 (0.6)

Values in parenthesis are standard deviations

2.2. Model calculation for obtaining the hydration structure around S1

To evaluate the relative contrast of the hydration shell around S1 and obtain the structure of S1, global search for the orientation of the lever arm and the contrast of the hydration shell was performed. Figure 2A shows the contrast-dependence of the score function, P of equation (1) in a range between 0% and 20%. (The range above 20% was omitted because of monotonic increase in P with increasing the contrast.) P has a rather flat region in a range between 10% and 15% with the minimum at 14%. Figure 2B shows the comparison of the experimental scattering curves and the scattering curves calculated from the model at the minimum P. The good fits to the experimental curves were obtained in the range of $0.015 < Q < 0.15$ Å^{-1}. The values of the residual χ^2 of equation (4) of this model were 1.24 for SAXS, 1.02 for SANS in H_2O, and 1.88 for SANS in D_2O. The R_g values of the models were 40.6 Å for SAXS, 39.3 Å for SANS in H_2O, and 38.5 Å for SANS in D_2O. These R_g values were within a range of one standard deviation of the measured R_g values (see Table 1). For the models at the contrasts out of the range between 10% and 15%, at least
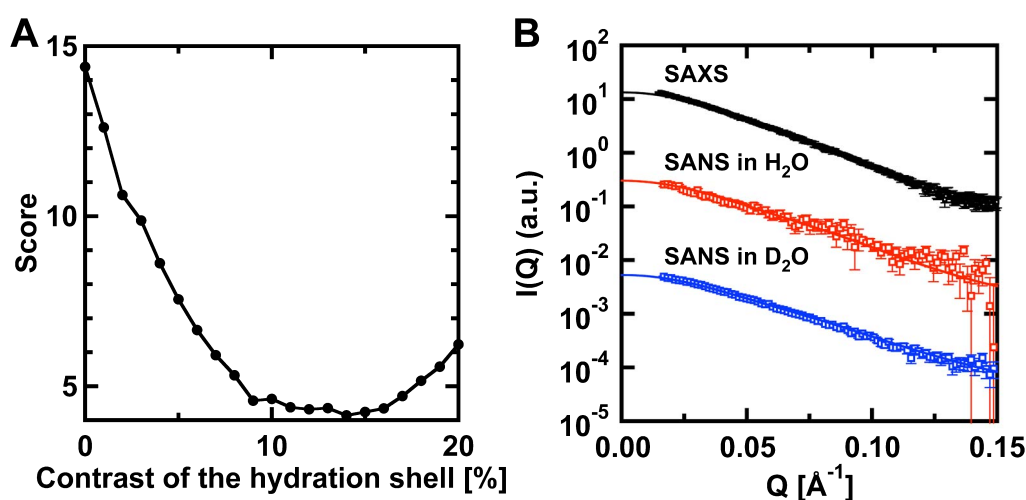
Figure 2 (A) Dependence of the score function, P, on the contrast of the hydration shell. (B) Comparison of the experimental scattering curves with the calculated scattering curves of the best model at 14% contrast. Open squares and solid lines denote the experimental and calculated scattering curves, respectively. The curves are shifted vertically for clarity.

one of the χ^2 values became larger than 2.0 in addition to worse values of P, indicating that the simultaneous fits to the scattering curves failed at the contrasts below 10% and above 15%. The acceptable range of the contrast was thus between 10% and 15%, consistent with the earlier result that S1 had usual hydration water[31]. An ensemble of the models in the acceptable range of the contrast shows different orientations of the lever arm from that of the crystal structure, though such a difference was not observed in the earlier study[26]. The origin of this discrepancy is not clear at present. Slight differences in the conditions for chymotrypsin treatment, however, may have caused digestion of a few more residues in the motor domain, which could unstabilize the interaction between the lever arm and the motor domain at their junction and thereby changing the orientation of the lever arm as detected here. Such a local perturbation is unlikely to modify the overall hydration structure significantly.

2.3. Model calculation for obtaining the hydration structure around F-actin

The R_c values of F-actin for SAXS, SANS in H_2O, and SANS in D_2O were calculated at each of the contrasts between 0% and 50% with a step of 1%, using the atomic models of F-actin. The contrast-dependence of these R_c values obtained from the calculations is shown in Figure 3A. Although these calculations were performed using the 13-mers or 12-mers of the F-actin models, such calculations using the 10-mers, 26-mers and 39-mers of the F-actin models confirmed that the R_c values did not depend on the number of monomers (data not shown). Figure 3B shows the contrast-dependence of the score function, S of equation (5) calculated from these R_c values. The model based on the EM structure of 3MFP (3MFP-EM) reached the minimum value of S at the contrast of 20%, at which the R_c values are

25.4 Å for SAXS, 24.1 Å for SANS in H_2O, and 22.8 Å for SANS in D_2O. These values are within a range of one standard deviation of the corresponding experimental R_c values. On the other hand, the model based on the XFD structure of 2ZWH (2ZWH-XFD) reached the minimum value of S at the contrast of 36%, at which the R_c values are 25.4 Å for SAXS, 23.4 Å for SANS in H_2O, and 21.6 Å for SANS in D_2O. Another model based on the EM structure of 3G37 (3G37-EM) reached the minimum at the contrast of 40%, at which the R_c values are 25.4 Å for SAXS, 23.2 Å for SANS in H_2O, and 20.9 Å for SANS in D_2O. The R_c values of the 2ZWH-XFD and 3G37-EM models are also within a range of one standard deviation of the experimental values except for the values from SANS in D_2O. Assuming that the acceptable range of the calculated R_c values are within twice the standard deviations of the experimental values, the acceptable range of the contrast was between 19% and 21% for the 3MFP-EM model, and between 34% and 38% for the 2ZWH-XFD model. The fits using the 3G37-EM model did not satisfy this criterion because the R_c value from SANS in D_2O was out of the range of twice the standard deviation.

The atomic models of F-actin used here should be free from the distorting molecular force. The difference in the optimal contrast of the hydration shell among these models arises from slight differences in their conformations as shown in Figure 4. When F-actin models used in this study are helically projected onto the plane perpendicular to the fiber axis and viewed from the pointed-end, the 3MFP-EM model is shown to be more expanded as a whole than the 2ZWH-XFD model although the centers of mass of these models virtually coincide with each other (Fig. 4A). On the other hand, the 3G37-EM model is the closest to the fiber axis among these three models, and the relative position of the inner and the outer domains within an actin monomer is slightly different from that in other two models (Fig. 4B and
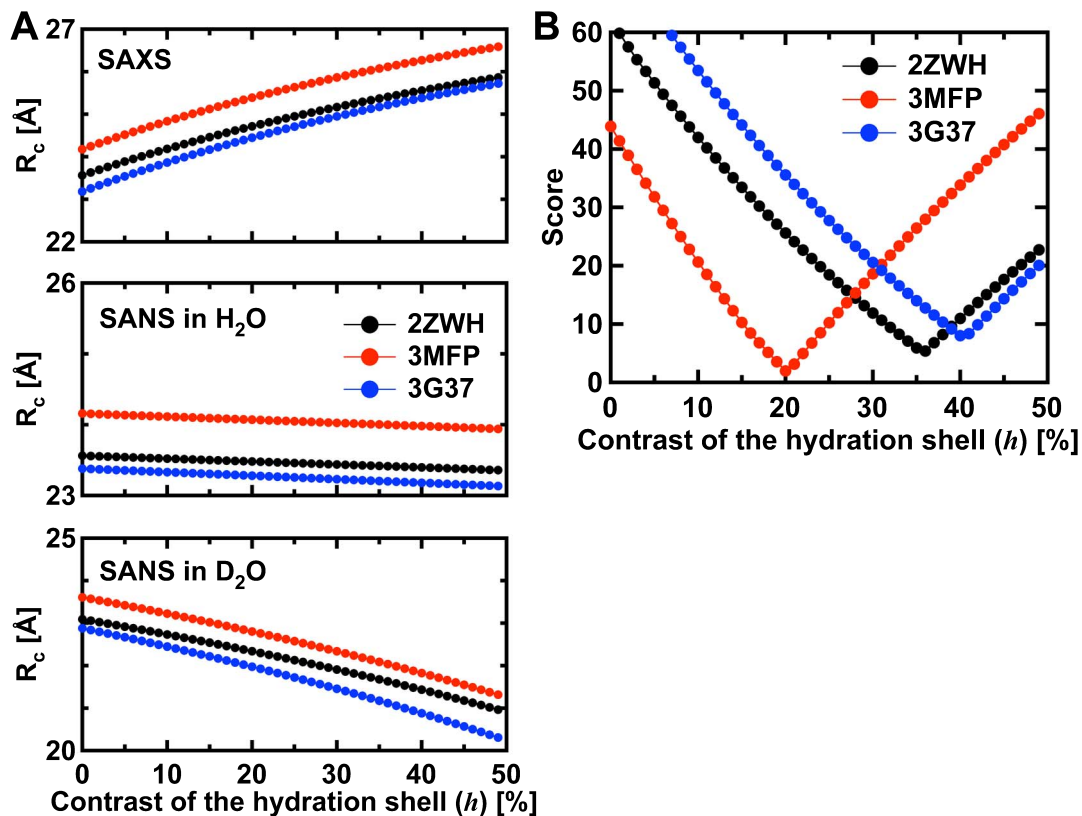
Figure 3 (A) Dependence of the R_c values of the F-actin models on the contrast of the hydration shell. The calculated R_c values based on the models of 2ZWH-XFD, 3MFP-EM and 3G37-EM are shown. (B) Dependence of the score function, S, on the contrast of the hydration shell. The values of S of the models of 2ZWH-XFD, 3MFP-EM and 3G37-EM are shown.

C). F-actin was demonstrated to have a range of structural conformations, which are distinct in local structures, but overall structures of which are similar to the 2ZWH-XFD model[32]. F-actin in solution is thus likely to have an ensemble of conformations similar to the three models above. Since the most expanded structure is that of the 3MFP-EM model, the relative contrast 19–21% higher than bulk water obtained from the modeling should be the minimum contrast. It is thus concluded that the contrast of the hydration shell around F-actin is at least 19% higher than bulk water and it could be more than 30%. This value is significantly higher than the value for S1.

Svergun et al. first applied the technique employed here to protein solutions and concluded that the hydration shell around the protein has on average the density ~10% higher than that of bulk water[7]. A molecular dynamics simulation study showed that the density of the hydration shell around hen egg white lysozyme is 15% higher than bulk water[33]. Furthermore, a recent analysis of small- and wide-angle X-ray scattering of protein solutions suggested that the contrast of the hydration shell around myoglobin is about 10%[34], and solvent analysis of insulin crystal showed the hydration shell with 10% higher density than bulk water[35]. Taking these and other evidences into consideration, the first hydration shell around the proteins is considered to

have an average density of at most 10% higher than that of bulk water[36]. The results of the hydration shell around S1 obtained here fit into this general picture. On the other hand, F-actin, having the hydration shell with more than 19% higher density than bulk water, is out of this picture. F-actin thus has an unusual hydration structure.

This hydration structure around F-actin could be interpreted as follows. F-actin has been shown to have clusters of negative charges on the solvent-accessible surface[37]. These negative charges produce the electric field, the strength of which is comparable to that around an iodide ion[6]. An iodide ion has been shown to make the water structure around the ion highly disordered[38]. Furthermore, the number of hydrogen-bonds per water molecule is significantly reduced around the iodide ion compared to bulk water[39]. Such disordered water structure increases the density of the hydration shell. The clusters of the negative charges around F-actin should thus have the similar effects of making the water structure disordered and thereby increasing the density of the hydration shell.

In such a disordered hydration shell, each water molecule may rotate more rapidly than that in bulk water despite of high density because of the disrupted hydrogen-bond network. The hydration shell with high density around F-actin could thus be related to the unusual behavior of the water
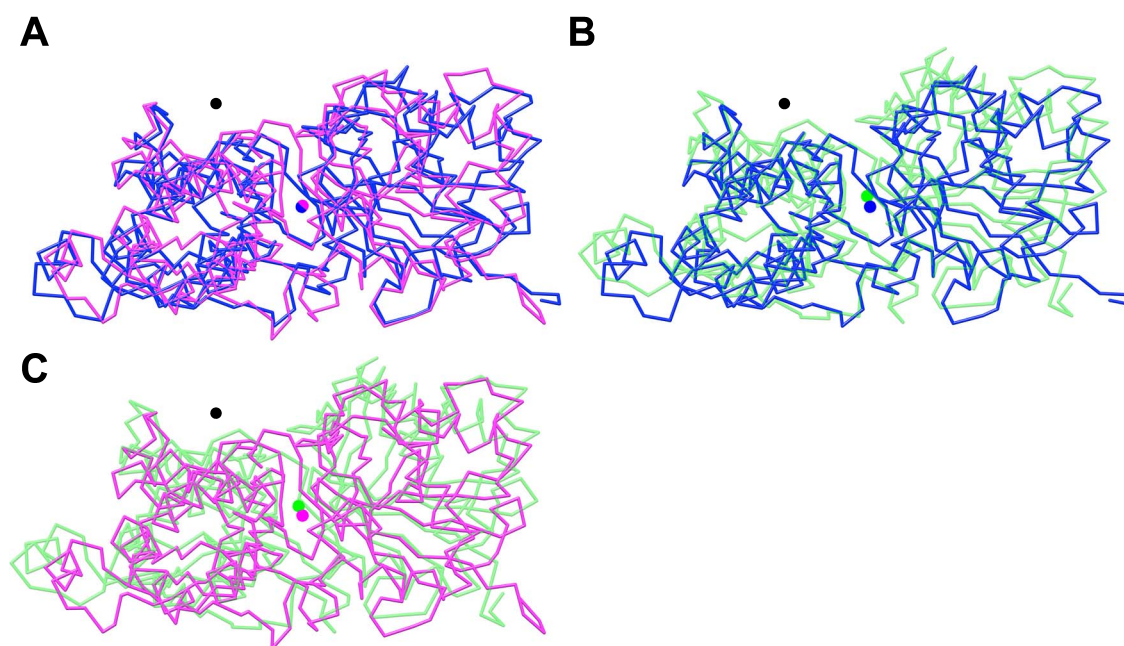
Figure 4 Comparisons of the structures of the F-actin models helically projected onto the plane perpendicular to the fiber axis, viewed from the pointed end of F-actin. The models of 2ZWH-XFD, 3MFP-EM and 3G37-EM are shown in magenta, blue and light green, respectively. The centers of mass of these projected structures are shown in filled circles in corresponding colors. The fiber axis is denoted by a filled circle in black. (A) Comparison of 2ZWH-XFD and 3MFP-EM models. (B) Comparison of 3G37-EM and 3MFP-EM models. (C) Comparison of 3G37-EM and 2ZWH-EM models. The diagrams were drawn using UCSF Chimera[41].

molecules around F-actin, which was suggested by a microwave dielectric spectroscopic study[6] that the water molecules around F-actin have higher rotational mobility than bulk water (the hyper-mobile water, HMW). The results of the earlier studies showing that the HMW was detected around iodide ions[6] but not around the proteins having usual hydration water such as S1, myoglobin, and lysozyme[31,40] may be in concert with the relevance of the unusual density of the hydration shell to the HMW.

The results obtained here indicate that the hydration structures were different between F-actin and myosin S1, which are counterparts in muscle contraction. Changes in the hydration structure would play important roles in protein-protein interactions, as suggested for the acto-S1 interaction.[6,31] Systematic studies on hydration water around various proteins are required to elucidate the roles which hydration water plays in a variety of protein functions.

Acknowledgements

REFERENCES

1. Fujiwara, S., Plazanet, M., Matsumoto, F. & Oda, T. Differences in internal dynamics of actin under different structural states detected by neutron scattering. *Biophys. J.* **94**, 4880–4889 (2008).
2. Fujiwara, S., Plazanet, M., Matsumoto, F. & Oda, T. Internal motions of actin characterized by quasielastic neutron scattering. *Eur. Biophys. J.* **40**, 661–671 (2011).
3. Fujiwara, S., Plazanet, M. & Oda, T. Coupling of the hydration water dynamics and the internal dynamics of actin detected by quasielastic neutron scattering. *Biochem. Biophys. Res. Comm.* **431**, 542–546 (2013).
4. Pollard, T. D., Blanchoin, L. & Mullins, R. D. Molecular mechanisms controlling actin filament dynamics in nonmuscle cells. *Annu. Rev. Biophys. Biomol. Struct.* **29**, 545–576 (2000).
5. Yamada, T. & Sugi, H. Nuclear magnetic resonance spectroscopy of skeletal muscle and muscle proteins. *Jpn. J. Physiol.* **46**, 201–213 (1996).
6. Kabir, S. R., Yokoyama, K., Mihashi, K., Kodama, T. & Suzuki, M. Hyper-mobile water is induced around actin filament. *Biophys. J.* **85**, 3154–3161 (2003).
7. Svergun, D. I., Richard, S., Koch, M. H. J., Sayers, Z., Kuprin, S. & Zaccai, G. Protein hydration in solution: Experimental observation by x-ray and neutron scattering. *Proc. Natl. Acad. Sci. USA* **95**, 2267–2272 (1998).
8. Oda, T., Makino, K., Yamashita, I., Namba, K. & Maéda, Y. Effect of the length and effective diameter of F-actin on the filament orientation in liquid crystalline sols measured by x-ray fiber diffraction. *Biophys. J.* **75**, 2672–2681 (1998).
9. Coué, M. & Korn, E. D. Interaction of plasma gelsolin with G-actin and F-actin in the presence and absence of calcium ions. *J. Biol. Chem.* **260**, 15033–15041 (1985).

10. Weeds, A. G. & Taylor, R. S. Separation of subfragment-1 isoenzymes from rabbit skeletal muscle myosin. *Nature* **257**, 54–56 (1975).

11. Hammersley, A. P., Svensson, S. O., Hanfland, M., Fitch, A. N. & Häusermann, D. Two-dimensional detector software: from real detector to idealised image or two-theta scan. *High Pressure Research* **14**, 235–248 (1996).

12. Konarev, P. V., Volkov, V. V., Sokolova, A. V., Koch, M. H. J. & Svergun, D. I. PRIMUS—a Windows-PC based system for small-angle scattering data analysis. *J. Appl. Cryst.* **36**, 1277–1282 (2003).

13. Dewhurst, C. GRASP, http://www.ill.eu/instruments-support/instruments-groups/groups/lss/grasp/ (2002).

14. Feigin, L. A., Svergun, D. I. *Structure Analysis by Small-Angle X-ray and Neutron Scattering* (Plenum Press, New York and London, 1987).

15. Rayment, I., Rypniewski, W. R., Schmidt-Bäse, K., Smith, R., Tomichick, D. R., Benning, M. M., Winkelmann, D. A., Wesenberg, G. & Holden, H. M. Three-dimensional structure of myosin subfragment-1: a molecular motor. *Science* **261**, 50–58 (1993).

16. Fernandez-Fuentes, N., Zhai, J. & Fiser., A. ArchPRED: a template based loop structure prediction server. *Nucleic Acids Res.* **34**, 173–176 (2006).

17. Sugimoto, Y., Sato, O., Watanabe, S., Ikebe, R., Ikebe, M. & Wakabayashi, K. Reverse conformational changes of the light chain-binding domain of myosin V and VI processive motor heads during and after hydrolysis of ATP by small-angel x-ray solution scattering. *J. Mol. Biol.* **392**, 420–435 (2009).

18. Houdousse, A., Szent-Györgyi, A. G. & Cohen, C. Three conformational states of scallop myosin S1. *Proc. Natl. Acad. Sci. USA* **97**, 11238–11243 (2000).

19. Reconditi, M., Koubassova, N., Linari, M., Dobbie, I., Narayanan, T., Diat, O., Piazzesi, G., Lombardi, V. & Irving, M. The conformation of myosin head domains in rigor muscle determined by x-ray interference. *Biophys. J.* **85**, 1098–1110 (2003).

20. Svergun, D., Barberato, C. & Koch, M. H. J. CRYSOL—a program to evaluate x-ray solution scattering of biological macromolecules from atomic coordinates. *J. Appl. Cryst.* **28**, 768–773 (1995).

21. Oda, T., Iwasa, M., Aihara, T., Maéda, Y. & Narita, A. The nature of the globular- to fibrous-actin transition. *Nature* **457**, 441–445 (2009).

22. Fujii, T., Iwane, A. H., Yanagida, T. & Namba, K. Direct visualization of secondary structures of F-actin by electron cryomicroscopy. *Nature* **467**, 724–728 (2010).

23. Murakami, K., Yasunaga, T., Noguchi, Q. P. T., Gomibuchi, Y., Ngo, K. X., Uyeda Q. P. T. & Wakabayashi, T. Structural basis for actin assembly, activation of ATP hydrolysis, and delayed phosphate release. *Cell* **143**, 275–287 (2010).

24. Matsuo, T., Ueno, Y., Takezawa, Y., Sugimoto, Y., Oda, T., Wakabayashi, K. X-ray fiber diffraction modeling of structural changes of the thin filament upon activation of live vertebrate skeletal muscles. *BIOPHYSICS* **6**, 13–26 (2010).

25. Garrigos, M., Mallan, S., Vachette, P. & Bordas, J. Structure of the myosin head in solution and the effect of light chain 2 removal. *Biophys. J.* **63**, 1462–1470 (1992).

26. Arata, T., Kimura, S., Sugimoto, Y., Takezawa, Y., Iwasaki, N. & Wakabayashi, K. Structure of the monomeric actin-myosin head complex as revealed by X-ray solution scattering. *Adv. Exp. Med. Biol.* **453**, 73–78 (1998).

27. Mendelson, R. A., Bivin, D., Curmi, P. M. G., Schneider, D. K. & Stone, D. B. Recent neutron scattering studies of muscle contraction and its control. *Adv. Biophys.* **27**, 143–153 (1991).

28. Whitten, A. E., Jeffries, C. M., Harris, S. P. & Trewhella, J. Cardiac myosin-binding protein C decorates F-actin: implications for cardiac function. *Proc. Natl. Acad. Sci. USA* **105**, 18360–18365 (2008).

29. Matsudaira, P., Bordas, J. & Koch, M. H. J. Synchrotron x-ray diffraction studies of actin structure during polymerization. *Proc. Natl. Acad. Sci. USA* **84**, 3151–3155 (1987).

30. Lepault, J., Ranck, J. L., Erk, I. & Carlier, M. F. Small angle x-ray scattering and electron cryomicroscopy study of actin filaments: role of the bound nucleotide in the structure of F-actin. *J. Struct. Biol.* **112**, 79–91 (1994).

31. Suzuki, M., Kabir, S. R., Siddique, M. S. P., Nazia, U. S., Miyazaki, T. & Kodama, T. Myosin-induced volume increase of the hyper-mobile water surrounding actin filaments. *Biochem. Biophys. Res. Commun.* **322**, 340–346 (2004).

32. Galkin, V. E., Orlova, A., Schröder, G. F. & Egelman, E. H. Structural polymorphism in F-actin. *Nat. Struct. Mol. Biol.* **17**, 1318–1323 (2010).

33. Merzel, F. & Smith, J. C. Is the first hydration shell of lysozyme of high density than bulk water? *Proc. Natl. Acad. Sci. USA* **99**, 5378–5383 (2002).

34. Virtanen, J. J., Makowski, L., Sosnick, T. R. & Freed, K. F. Modeling the hydration layer around proteins: applications to small- and wide-angle x-ray scattering. *Biophys. J.* **101**, 2061–2069 (2011).

35. Badger, J. & Caspar, D. L. D. Water structure in cubic insulin crystals. *Proc. Natl. Acad. Sci. USA* **88**, 622–626 (1991).

36. Makarov, V., Pettitt, B. M. & Feig, M. Solvation and hydration of proteins and nucleic acids: a theoretical view of simulation and experiment. *Acc. Chem. Res.* **35**, 376–384 (2002).

37. Ouporov, I. V., Knull, H. R., Thomasson, K. A. Brownian dynamics simulations of interactions between aldolase and G- or F-actin. *Biophys. J.* **76**, 17–27 (1999).

38. Tongraar, A., Hannongbua, S. & Rode, B. M. QM/MM MD simulations of iodide ion (I⁻) in aqueous solution: a delicate balance between ion-water and water-water H-bond interactions. *J. Phys. Chem. A* **114**, 4334–4339 (2010).

39. Heuft, J. M. & Meijer, E. J. Density functional theory based molecular-dynamics study of aqueous iodide solvation. *J. Chem. Phys.* **123**, 94506 (2005).

40. Yokoyama, K., Kamei, T., Minami, H. & Suzuki, M. Hydration study of globular proteins by microwave dielectric spectroscopy. *J. Phys. Chem. B* **105**, 12622–12627 (2001).

41. Pettersen, E. F., Goddard, T. D., Huang, C. C., Couch, G. S., Greenblatt, D. M., Meng, E. C. & Ferrin, T. E. UCSF Chimera —a visualization system for exploratory research and analysis. *J. Comput. Chem.* **25**, 1605–1612 (2004).